Alloying effect on the electronic structures of Nb and Mo

1994 J. Phys.: Condens. Matter 6 5081

(http://iopscience.iop.org/0953-8984/6/27/017)

J. Phys.: Condens. Matter 6 (1994) 5081–5096. Printed in the UK

Alloying effect on the electronic structures of Nb and Mo

Satoshi Inoue†, Jun-ichi Saito†, Masahiko Morinaga† and Shigeki Kano‡

† Department of Production Systems Engineering, Toyohashi University of Technology, Toyohashi, Aichi 441, Japan

‡ O-arai Engineering Centre, Power Reactor and Nuclear Fuel Development Corporation, O-arai-cho, Higashi-Ibaraki-gun, Ibaraki 311-13, Japan

Received 18 November 1993

Abstract. The alloying effects on the electronic structure were investigated for both Nb-based and Mo-based alloys in order to obtain useful information for alloy design. The electronic structure was calculated using the DV-Xα cluster method, and two alloying parameters, the bond order BO and the d-orbital energy level MD, were obtained for a variety of alloying elements M in these metals. The binary phase diagrams of the Nb–M and Mo–M systems were found to be classified according to the location in the BO–MD map. Also, with respect to the nature of the chemical bond between atoms, Nb and Mo were compared with the other BCC metals such as Ti, V, Cr, Fe and Zr. Furthermore, it was shown that the activation energy for atomic diffusion, the heat of fusion and the melting temperature could be associated with the bond order. These results will indeed give some guide to the design of these refractory-metal-based alloys for high-temperature applications.

1. Introduction

Niobium and molybdenum are 4d transition metals, having a body-centred cubic (BCC) lattice. Recently, great attention has been directed towards these Nb-based and Mo-based alloys (e.g. Nb–1 wt.% Zr and TZM (Mo–0.5 wt.% Ti–0.5 wt.% Zr) [1]), because of the high potential for a variety of structural applications at high temperatures. In fact, some alloys which possess a high heat resistance and also excellent mechanical properties at elevated temperatures have been developed for structural applications in advanced nuclear power systems (e.g. a portable fast breeder reactor system) [2].

However, despite extensive studies on refractory-metal-based alloys including both Nb-based and Mo-based alloys, alloying behaviour has not been well understood as yet. Most previous studies have been devoted to the magnetic state of 3d impurity elements (e.g. Fe and Mn) in Nb and Mo [3–12]. In general there is good agreement between the electronic structures of pure Nb and Mo from several band calculations [3, 10, 11], but the calculations involving alloying elements [3, 8] are so limited that there are many difficulties in evaluating alloying behaviour in a systematic manner. Miedema [13] has proposed an empirical method for treating the heat of formation for intermetallic compounds using two parameters: electronegativity and electron density at the Wigner–Seitz cell boundary. However, it is still uncertain that this method is applicable to the phase stability of disordered alloys, even though Chelikowsky [14] has employed these parameters to predict the solid solubility of magnesium alloys.

Therefore, what is really needed is first to estimate the alloying effect of elements on the physical properties of Nb and Mo by using the proper method. Needless to say, most alloy properties are very sensitive to the electronic state, and hence it is desirable

0953-8984/94/275081+16$19.50

to make an electronic approach to this alloy problem. In fact, we have shown recently that molecular orbital calculations are very useful in determining new parameters which represent the alloying behaviour of elements in various transition-metal-based alloys [15–21]. For example, a solid solubility limit could be predicted accurately with such parameters [20,21]. Therefore, this theoretical approach is worth applying to both the Nb-based and the Mo-based alloys, for which there are some difficulties in doing experiments because of their high melting temperatures.

In this study, in order to obtain useful information for alloy design, alloying effects on the electronic structures of Nb and Mo were calculated systematically by the DV-Xα cluster method. The thermal properties and the binary phase diagrams of Nb and Mo were elucidated, employing the calculated results. Also, the results were compared with those of Ti, V, Cr, Fe and Zr metals, all of which have a BCC lattice as do Nb and Mo.

2. DV-Xα method and cluster model

The DV-Xα cluster method [22,23] is a molecular orbital method, assuming the Hartree–Fock–Slater approximation. In this calculation, the exchange–correlation between electrons is given by the following Slater's Xα potential:

$$V_{xc} = -3\alpha\left[\frac{3}{8\pi}\rho(r)\right]^{-1/3}$$

where $\rho(r)$ is the density of electrons at position r, the parameter α is fixed at 0.7 and the self-consistent change approximation is used in this calculation. The matrix elements of the Hamiltonian and the overlap integrals are calculated by a random sampling method. The molecular orbitals are constructed by a linear combination of numerically generated atomic orbitals. The atomic orbitals used in this study were 1s–5p for Nb and Mo. Also, for alloying elements explained below, they were 1s–3p for Al and Si and 1s–np for transition metals ($n = 4$ for 3d transition metals; $n = 5$ for 4d transition metals; $n = 6$ for 5d transition metals).

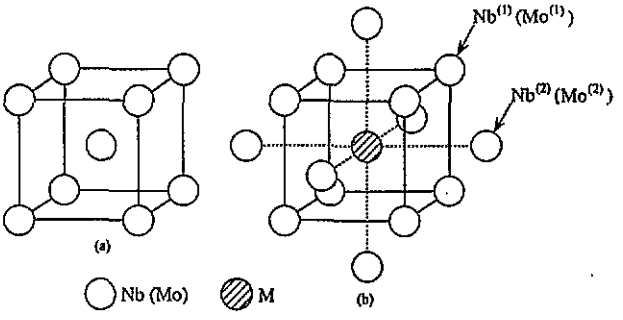

Figure 1. (a) Crystal structure of BCC Nb and Mo and (b) cluster model, MNb_{14} or MMo_{14} used in the calculation.

The crystal structure and the cluster model used in the calculation are shown in figures 1(a) and (b) respectively. As shown in figure 1(b), both the MNb_{14} and the MMo_{14}

clusters consisted of a central alloying element M and the surrounding first- and second-nearest-neighbour base-metal atoms. The alloying elements M chosen for this calculation were Al, Si (non-transition metals), Ti, V, Cr, Mn, Fe, Co, Ni and Cu (3d transition metals), Zr, Nb, Mo and Tc (4d transition metals), and Hf, Ta, W, Re (5d transition metals). In addition, Ru, Rh, Pd, Ag (4d transition metals) and Os, Ir, Pt, Au (5d transition metals) were chosen as the alloying elements in Nb. The lattice constants used were 0.330 66 nm for Nb and 0.314 69 nm for Mo, the same values as in the bulk.

The bond order BO which shows the overlap population of electrons between atoms was calculated following the Mulliken [24] population analysis. This is a measure of the strength of the covalent bond between atoms. The electron densities of states were also calculated from the energy level structure using the overlapping Gaussian functions which have a width of 0.2 eV and their centres located at each cluster energy level [25]. In addition, the d-orbital energy levels MD of alloying elements were obtained from the energy level structure of the cluster. As explained later, the parameter MD was associated with the atomic radius and the electronegativity of elements. The alloying behaviour was examined with the aid of these calculated results.

Furthermore, for comparison, using the same method, electronic structures were calculated for the pure BCC metals Ti, V, Cr, Fe and Zr. Here, the atomic orbitals used were 1s–4p for Ti, V, Cr and Fe, and 1s–5p for Zr, and the lattice constants were 0.332 01 nm, 0.302 32 nm, 0.288 45 nm, 0.286 60 nm and 0.360 91 nm for Ti, V, Cr, Fe and Zr, respectively.

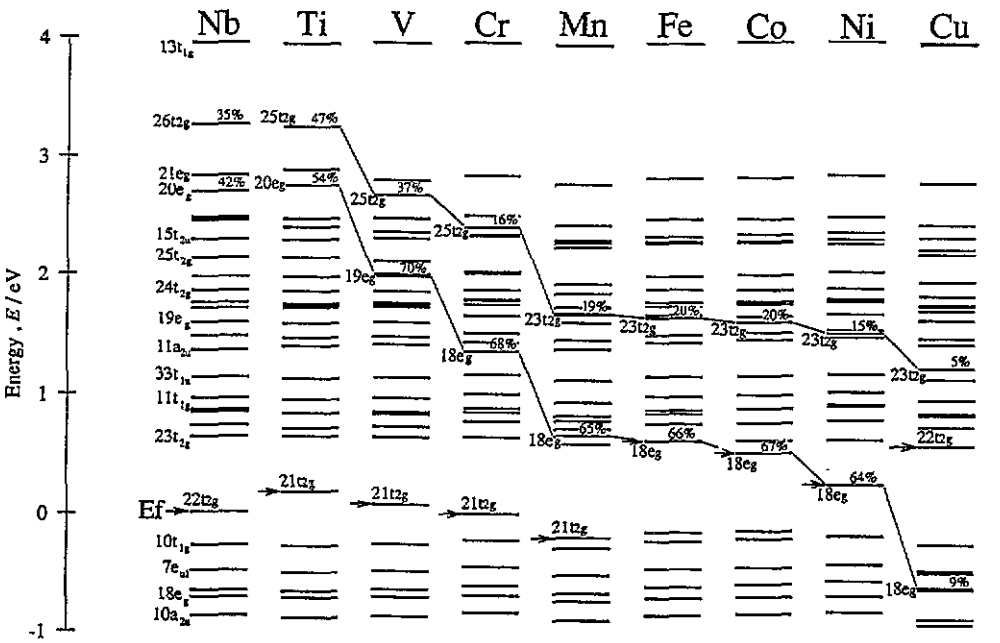

Figure 2. Energy level structures for pure Nb and alloyed Nb with 3d transition elements.

3. Results

3.1. Energy level structure and d-orbital energy level

The energy level structures are shown in figure 2 for pure Nb and for the Nb containing 3d transition metals Ti, V, Cr, Mn, Fe, Co, Ni and Cu. They were drawn by setting the Fermi energy level of pure Nb to zero, and the Fermi energy level E_F for each cluster is indicated by an arrow in the figure. The 3d component of a central alloying transition element appeared in the t_{2g} and the e_g levels because of the O_h symmetry of the cluster. Since the d–d covalent interaction is most significant in transition metals, both the t_{2g} and the e_g levels are considered to be the levels characteristic of alloying elements. The fractions of the 3d component in each energy level are listed in table 1. The representative energy level for each alloying element was supposed to be that which has the largest fraction, and it changed monotonically with the atomic number as shown in figure 2. However, in some cases the 3d component was split over several energy levels. For example, as shown in table 1, in the case of the Cr addition, the percentages of the Cr 3d component in the $24t_{2g}$ and the $25t_{2g}$ levels, were 15.6 and 16.1%, respectively, indicating that the d component appeared evenly in both energy levels. Therefore, the average t_{2g} level was calculated by taking a weighted average of the d component in the $(22–25)t_{2g}$ levels (the $(23–26)t_{2g}$ levels for pure Nb), all of which existed above the Fermi energy level. Similarly, the average e_g level was calculated using the $(18–20)e_g$ levels (the $(19–21)e_g$ levels for pure Nb). Then, the d-orbital energy level MD was obtained by taking further a weighted average of these t_{2g} and e_g levels. In this weighting, the degeneracy of each level was taken into account. MD calculated in this way changed, following the order of elements in the periodic table, as shown in figure 3(b). Similar calculations of MD were also performed for Mo.

Table 1. Percentages of the 3d component of alloying element in the t_{2g} and e_g orbitals.

	Nb	Ti	V	Cr	Mn	Fe	Co	Ni	Cu
$26t_{2g}$	34.7								
$25t_{2g}$	1.3	46.8	36.7	16.1	3.8	2.9	2.0	1.2	0.3
$24t_{2g}$	0.3	15.6	5.4	15.6	2.7	1.1	0.4	0.1	0
$23t_{2g}$	0.6	0.4	0.9	3.3	18.6	19.7	19.3	15.5	5.0
$22t_{2g}$		1.3	1.1	0.9	0.8	0.8	0.7	0.6	0.3
$21e_g$	15.1								
$20e_g$	42.2	53.7	0.3	0.1	0	0	0	0	0
$19e_g$	0.3	15.4	69.6	2.1	0.2	0.1	0.1	0	0
$18e_g$		0.2	1.5	67.7	65.0	65.6	67.1	63.7	9.3

As shown in figure 3(a), MD tends to increase with increasing atomic radius of alloying element M. This is simply due to the weaker interaction operating between electrons and the nucleus with increasing distance between them, resulting in the appearance of a higher MD in the level structure. In addition, as shown in figure 3(a), MD increases with decreasing electronegativity values of elements except for Cu, Ag and Au [17, 20, 26]. In fact, it is known that the eigenvalue obtained by the Xα calculation reflects the electronegativity itself [24].

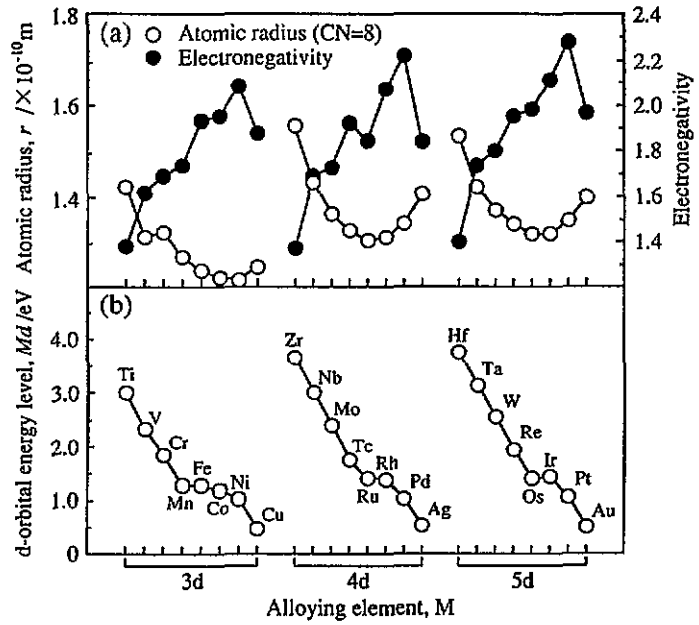

Figure 3. (a) Atomic radius (CN, 8) and electronegativity of alloying elements, and (b) changes in d-orbital energy level (MD) in Nb with alloying elements.

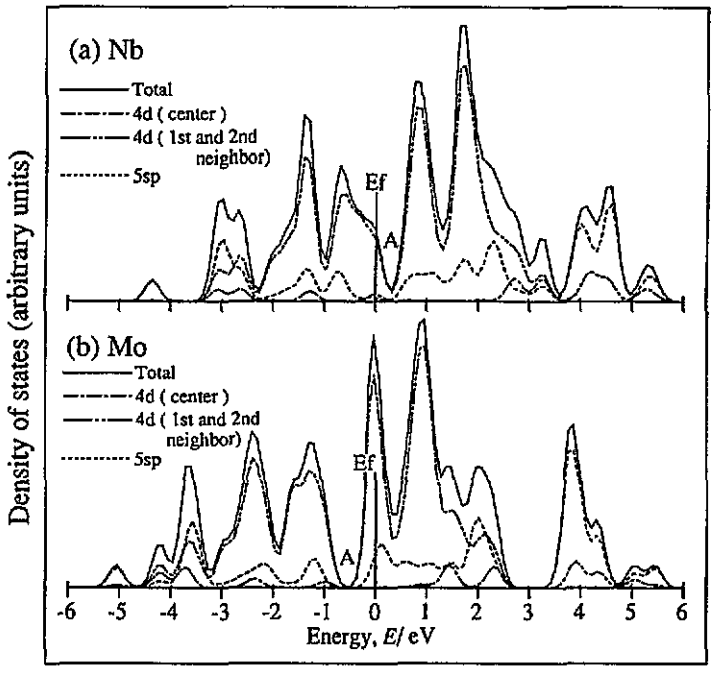

Figure 4. Electron density of states for (a) the Nb_{15} cluster and (b) the Mo_{15} cluster.

3.2. Electron density of states

The calculated electron densities of states are shown in figure 4(a) for pure Nb and in figure 4(b) for pure Mo. There was good agreement between the densities of states from the present calculation and the band calculations [3, 10, 11]. For example, a large valley existed in the energy band near the Fermi energy level E_F as is indicated by the letter A. This band separation is one of the characteristics of the electronic structure for BCC metals. Also, there were three small peaks in the lower-energy region below E_F [3]. In addition, the Fermi energy level lay in the 4d band for both pure Nb and pure Mo, and the component of 5s and 5p electrons extended to a wide energy range.

However, there was a little difference between the densities of states of pure Nb and pure Mo. The E_F of Nb existed on the lower-energy side of the large valley, but that of Mo existed on the higher-energy side. This is simply due to the larger number of valence electrons existing in Mo than in Nb.

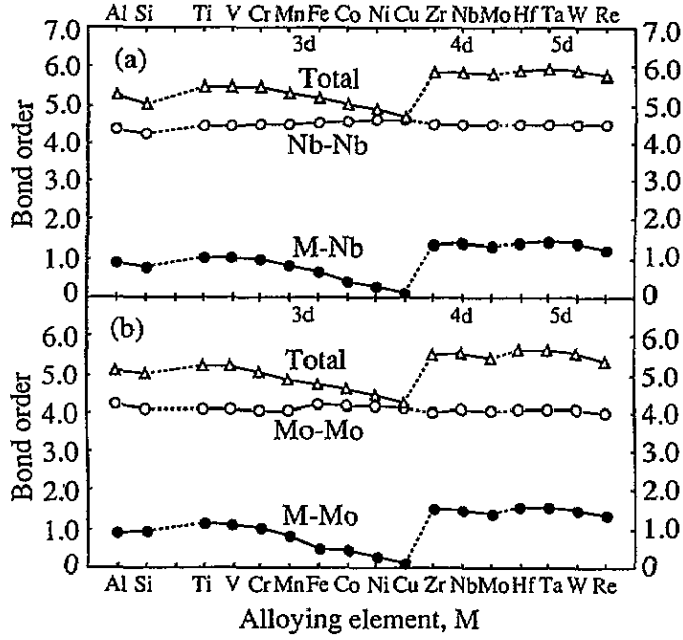

Figure 5. Changes in the bond order with alloying elements: (a) MNb_{14} cluster and (b) MMo_{14} cluster.

3.3. Bond order

The changes in the bond order with alloying elements M are shown in figure 5(a) for Nb and in figure 5(b) for Mo, and their respective values are also given in table 2 together with MD. As the d–d covalency is a major part of the total cohesive energy of transition metals and alloys, the bond order was calculated from the overlap populations of the d electrons between atoms in the cluster. In the figure, Nb–Nb (or Mo–Mo) indicates the bond order between the first-nearest-neighbour $Nb^{(1)}$ (or $Mo^{(1)}$) atoms and the second-nearest-neighbour $Nb^{(2)}$ (or $Mo^{(2)}$) atoms from a central M atom in the cluster. M–Nb (or M–Mo) indicates

Table 2. List of the BO and MD values for elements for Nb and Mo.

		M for Nb		M for Mo	
	M	BO	MD (eV)	BO	MD (eV)
3d	Ti	5.470	3.017	5.238	2.799
	V	5.481	2.319	5.212	1.893
	Cr	5.463	1.826	5.068	1.187
	Mn	5.319	1.287	4.849	0.781
	Fe	5.168	1.262	4.716	0.691
	Co	5.012	1.182	4.614	0.667
	Ni	4.901	1.015	4.459	0.265
	Cu	4.709	0.477	4.248	−0.307
4d	Zr	5.828	3.666	5.511	3.457
	Nb	5.867	2.999	5.578	2.651
	Mo	5.825	2.376	5.453	1.890
	Tc	5.659	1.744	5.236	1.237
	Ru	5.259	1.384		
	Rh	5.130	1.366		
	Pd	4.925	1.021		
	Ag	4.692	0.517		
5d	Hf	5.890	3.758	5.630	3.523
	Ta	5.930	3.139	5.642	2.819
	W	5.905	2.540	5.554	2.113
	Re	5.750	1.925	5.337	1.462
	Os	5.452	1.398		
	Ir	5.250	1.431		
	Pt	4.854	1.049		
	Au	4.707	0.484		
	Al	5.264	—	5.264	—
	Si	5.031	—	5.031	—

the bond order between the alloying element M and its first- and second-nearest-neighbour Nb (or Mo) atoms. Also, the curve labelled 'Total' denotes their sum.

Either the Nb–Nb or the Mo–Mo bond order scarcely varied with alloying elements. On the other hand, both the M–Nb and the M–Mo bond orders changed largely with alloying elements. For example, the Ti addition to Nb (or Mo) made the chemical bond stronger than the Cu addition. Also, the total bond order was higher for 4d and 5d transition metals than for 3d transition metals. Thus, the strength of chemical bonds between atoms was modified by alloying. It is also noticed here that there was a similar trend of the bond order changes with alloying elements between Nb and Mo.

3.4. Electron density difference map

The electrons density difference $\Delta\rho$ was calculated for alloyed Nb. Here, $\Delta\rho$ was defined as

$$\Delta\rho = \rho(\mathrm{MNb_{14}}) - \rho(\mathrm{NbNb_{14}})$$

where $\rho(\mathrm{MNb_{14}})$ and $\rho(\mathrm{NbNb_{14}})$ are the electron densities of the corresponding cluster denoted in parentheses. Therefore, this $\Delta\rho$ means the change in the spatial electron distribution in the cluster with alloying.

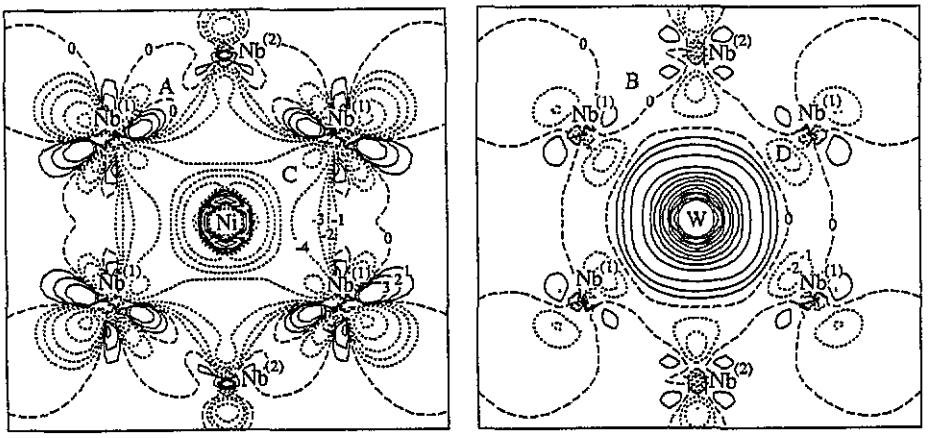

(a) Δρ(Nb-Ni) (b) Δρ(Nb-W)

Figure 6. Electron density difference maps on the (110) atomic plane for (a) Nb–Ni and (b) Nb–W where $0, \pm1, \pm2, \pm3, \pm4$ correspond to the electron density values $0, \pm0.002, \pm0.004, \pm0.008, \pm0.016$ (in electrons per atomic unit cubed), respectively.

The calculated electron density difference maps on the (110) atomic plane are shown in figure 6(a) for M ≡ Ni and in figure 6(b) for M ≡ W. In this figure, the region where $\Delta\rho > 0$ is indicated by full curves and the region where $\Delta\rho \leqslant 0$ is indicated by broken curves. Therefore, there are excess electrons in the region where $\Delta\rho > 0$, whereas deficient electrons in the region where $\Delta\rho \leqslant 0$. The appearance of a large positive or negative peak at the substitutional site is simply due to the difference between the total electron numbers of M and Nb atoms.

The changes in the bond orders with alloying elements shown in figure 5(a) could be understood from these electron density difference maps. For example, the electron density differences between the first- and the second-nearest-neighbour Nb atoms were almost zero regardless of alloying elements as is indicated by the two letters A and B in figures 6(a) and 6(b), in agreement with the little change in Nb–Nb bond order with alloying elements shown in figure 5(a). Also, the presence of a negative electron density difference region indicated by the letter C in figure 6(a) means that the Ni substitution for Nb atoms weakened the chemical bond strength in pure Nb. This also agreed with the result that the Nb–Ni bond order shown in figure 5(a) was smaller than the Nb–Nb bond order in pure Nb. On the other hand, a nearly unchanged region in the electron density difference extended between a central W and the first-nearest-neighbour Nb atoms as indicated by the letter *D* in figure 6(b). Thus, the Nb–W bond order and consequently the total bond order scarcely changed with the W addition, as is shown in figure 5(a).

4. Discussion

4.1. Thermal properties

4.1.1. Activation energies for impurity diffusion and for self-diffusion. It has been reported that the activation energy of impurities in BCC Ti increases linearly with increasing bond order [18]. In this case, the bond order is regarded as a parameter to represent the energy for cutting of the atomic bond necessary for impurity atoms to diffuse in metals. In figure 7, the

results are shown for Nb and Mo. The measured activation energies of various transition-metal impurities in Nb and Mo [27,28] changed linearly with the bond order except for Mo in Nb and for Ta in Mo.

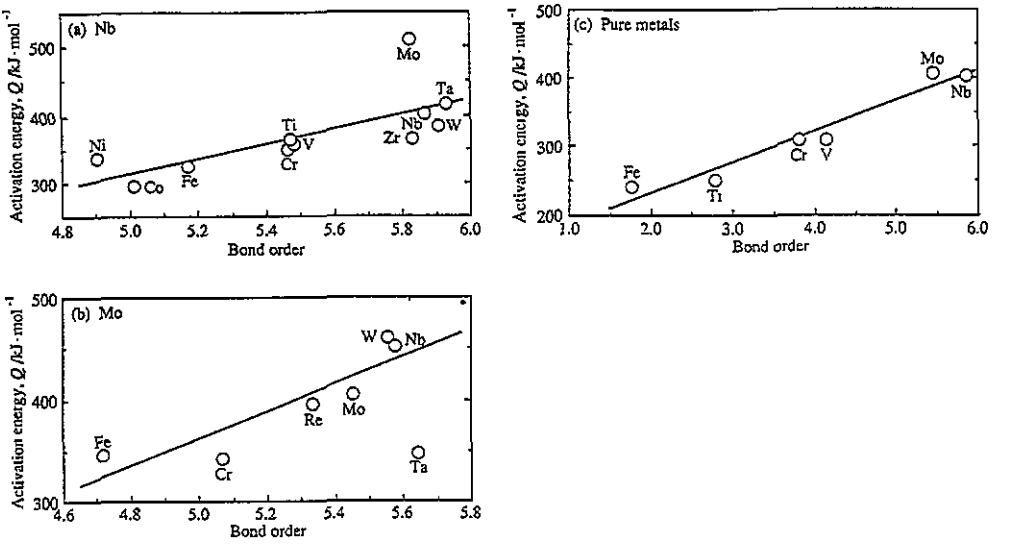

Figure 7. Correlation of the activation energies for impurity diffusion in (a) Nb and (b) Mo, and for self-diffusion in (c) pure metals with bond order.

It is interesting to note that commercial heat-resisting Mo-based alloys such as TZM and TZC contain Ti and Zr, both of which are elements of high bond order (see table 2) and hence of high activation energy for diffusion. The difficulty in atomic diffusion will lead to the super heat-resisting properties of these alloys, since the microstructure will be stable without any morphological change during the service at elevated temperatures.

Also, the activation energy for self-diffusion in pure BCC metals [27,28] correlated well with the bond order, as is shown in figure 7(c).

4.1.2. Heat of fusion and melting temperature. The bond orders of pure BCC metals are related to the heat of fusion and the melting temperature [27] as is shown in figure 8. The heat of fusion is the energy which is required for solid to transform into liquid at a melting temperature. Namely, it is expressed as the energy to relax chemical bonds in some ways during melting. As shown in figure 8, apparently the heat of fusion increased with increasing bond order, except for Cr. The melting temperature also increased with increasing bond order.

Creep resistance is one of the most important properties for the design of high-temperature materials. The creep of materials often takes place via atomic diffusion. Therefore, it is supposed that the creep resistance increases with increasing activation energy for atomic diffusion and also with increasing melting temperature. Thus, the present correlation shown in figures 7 and 8 may provide a clue to estimating the creep property of BCC metals and alloys at elevated temperatures.

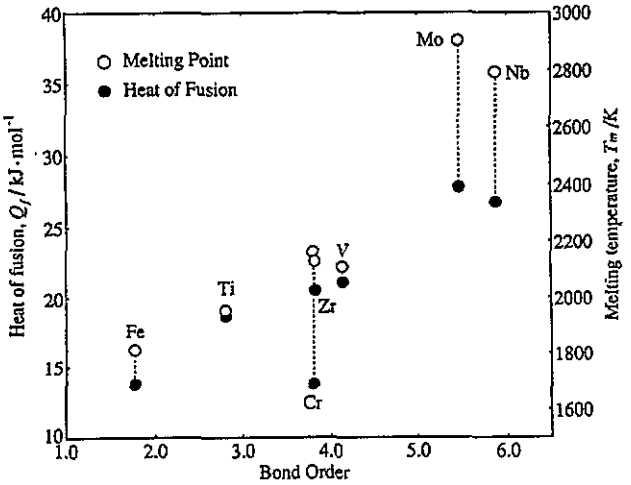

Figure 8. Correlation of the heat of fusion and melting temperature of pure metals with bond order.

4.2. Binary phase diagrams of Nb–M and Mo–M systems

4.2.1. Classification of binary phase diagrams. According to our previous study, it is known that both the d-orbital energy level, MD, and the bond order, BO are convenient parameters for describing the phase constitution in alloys [18]. This is because the parameters BO and MD are associated with the nature of the chemical bond between atoms in solids, through the covalency, electronegativity and atomic radius as explained before. In this study, these two parameters were also employed in order to classify the Nb–M and the Mo–M binary phase diagrams.

As is shown in figure 9, Nb (or Mo)–M binary phase diagrams [29] can be separated into the following four categories: the open circles represent the all-proportional solid solution system, the open triangles the all-proportional solid solution system but with a limited solid solubility at low temperatures because of the occurrence of the allotropic transformation in M, the full circles the eutectic system, and the full triangles the peritectic system.

The location of alloying elements on the BO–MD map is shown in figure 10(a) for Nb and in figure 10(b) for Mo. All the elements which form an all-proportional solid solution are located near the position of Nb or Mo on each map. This is reasonable because these elements are similar to Nb or Mo in the nature of the chemical bonds between atoms. The other elements having BO and MD with large differences from Nb or Mo are in the non-variant systems and some intermetallic phases appear in the phase diagram. It is interesting to note that there are only two eutectic systems in the Mo–M systems, Mo–Re and Mo–Tc systems, whereas the locations of Re and Tc in Mo are very near the position of the host element. This location may reflect an extent of the Mo-rich terminal solid solution wider than 40 mol% Re and 40 mol% Tc in the phase diagram [29], but no clear separation between eutectic and peritectic systems exists in the Nb–M systems on the map.

4.2.2. Intermetallic phases. There are intermetallic phases appearing next to the Nb (or Mo) terminal solid solution in the Nb–M (or Mo–M) binary non-variant systems. The M-to-Nb atomic compositional ratio for every compound phase is plotted as a function of L as shown in figure 11. Here, L is the distance from the position of Nb to

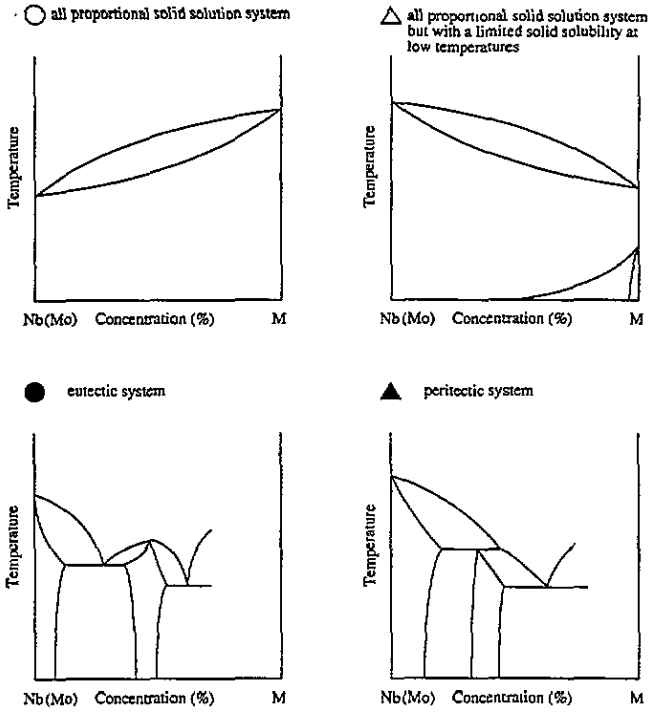

Figure 9. Classification of Nb–M (or Mo–M) binary phase diagrams.

the position of each alloying element M on the BO–MD map. This was calculated as $L = [(MD_M - MD_{Nb})^2 + (BO_M - BO_{Nb})^2]^{1/2}$. From this plot the $NbMn_2$ compound was omitted since the Nb–Mn phase diagram was not certain. As shown in figure 11, the M-to-Nb compositional ratios decrease with increasing distance L. Needless to say, the large L means that there is a significant difference in the characteristics of the elements from Nb or Mo. Obviously, it is difficult for these elements to exist stably in a terminal solid solution, but instead the second phases tend to form even at a low content of alloying elements. For example, in the case of Cr in Nb, L was as small as 1.24 and the compositional Cr-to-Nb ratio for the compound was as high as 2.00. However, in the case of Ni in Nb, L was as large as 2.03 and the compositional Ni-to-Nb ratio was as low as 0.86. This approach never explained which crystal structure is stable but predicted approximately alloy compositions where the second phase appears.

4.3. Comparison with other BCC metals

4.3.1. Bond order and energy distribution of the overlap populations. The comparison of the total bond order for a variety of pure BCC metals is shown in figure 12(a). The total bond order, which represents whole interactions between atoms in the cluster, decreased in the order Nb > Mo > V > Zr > Cr > Ti > Fe. Here, the order V > Cr > Ti > Fe for 3d transition metals was not the same as the order of elements in the periodic table. In figure 13, the energy distributions of the overlap populations between d-electrons are shown for Ti, V, Cr and Fe. In each figure, the Fermi energy level E_F was set to be zero. If the overlap population is positive (+), bonding-type interaction is operating between atoms whereas, if it is negative (−), anti-bonding-type interaction is dominant between atoms. The

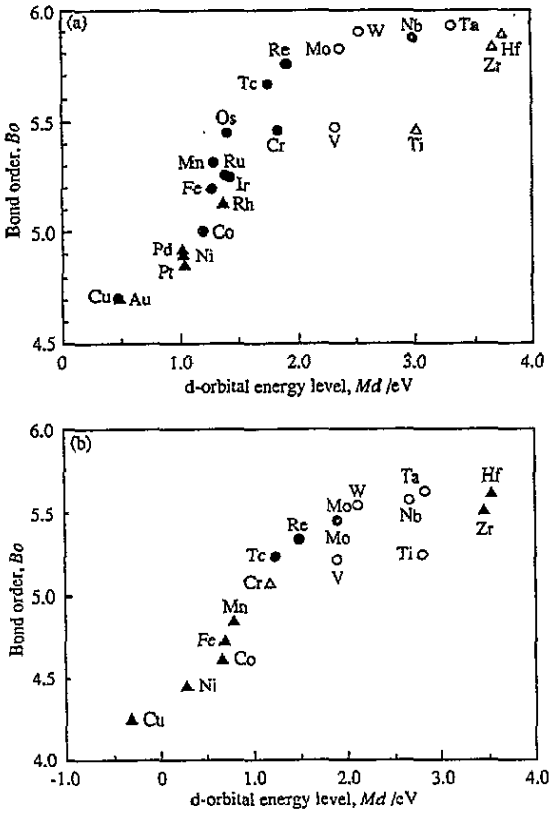

Figure 10. Location of alloying elements on the BO–MD map for (a) Nb and (b) Mo.

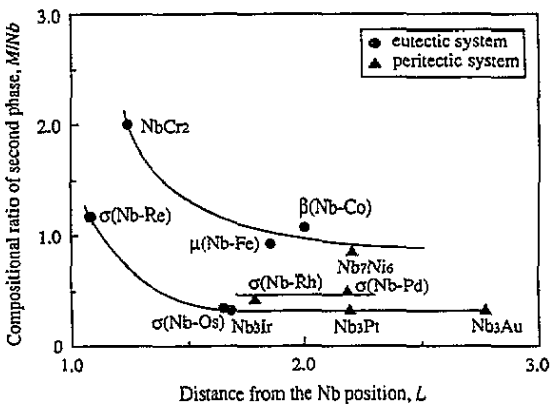

Figure 11. Relationship between the Nb–M distance L on the BO–MD map and the compositional ratio of second phases.

Fermi level of Ti was located in the bonding energy region where there was positive d–d bonding between atoms. The energy region where the bonding-type interaction is operating was filled gradually as the atomic number of metals increased and fully filled near V or Cr.

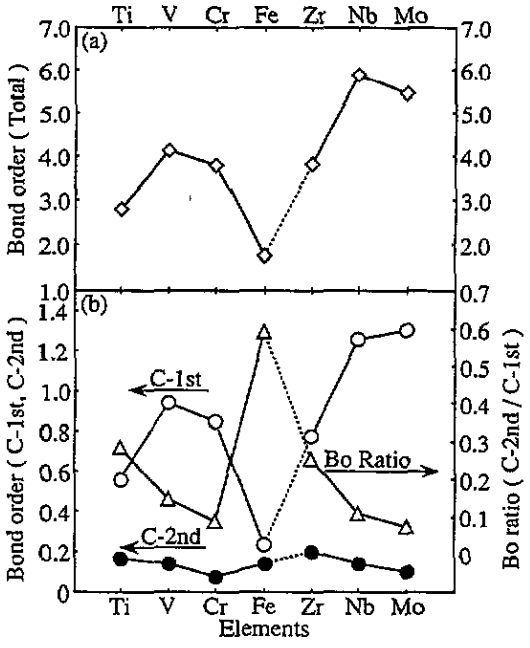

Figure 12. Comparison of (a) total bond order and (b) the first- or second-nearest-neighbour bond orders and the bond order ratio for several BCC metals.

As the E_F of Fe existed in the anti-bonding region, the d–d bonding was weaker in Fe than in other metals. As a result, the magnitude of the bond order changed following the order V > Cr > Ti > Fe.

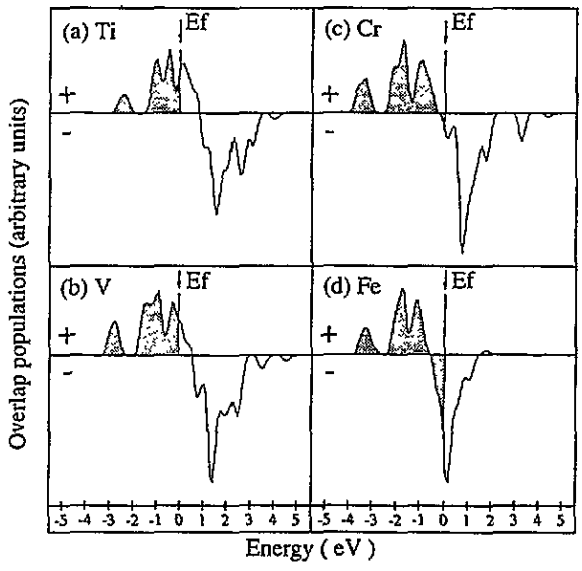

Figure 13. Changes in the d-electron overlap populations for (a) Ti, (b) V, (c) Cr and (d) Fe.

4.3.2. Allotropic transformation. From the structural point of view, the second-nearest-neighbour interatomic distance is only 15% larger than the first-nearest-neighbour distance in a BCC lattice. Therefore, as Pauling [30] has pointed out, the second-nearest-neighbour interaction is expected to be significant in BCC metals and alloys. In the case of the FCC lattice, the second-nearest-neighbour distance is 41% larger and hence such a second-neighbour interaction is less significant compared with the BCC lattice. However, this second-neighbour interaction differs considerably for the various BCC metals [17], and its magnitude is probably related to the structural stability of BCC metals. In order to discuss this problem further the bond order was utilized again here.

The bond order between a central atom and its surrounding atoms in a cluster is composed of two terms. One is the bond order between the central atom and the first-nearest-neighbour atoms (C–1st) and the other is the bond order between the central atom and the second-nearest-neighbour atoms (C–2nd). The magnitudes of C–1st and C–2nd bond orders and the (C–2nd) to (C–1st) ratio were compared for the various BCC metals [17] as is shown in figure 12(b). The C–1st bond order was much larger than the C–2nd bond order and is very sensitive to the metals. Also, the (C–2nd)-to-(C–1st) bond order ratio was dependent largely on the metals. For example, it was relatively large in the low C–1st bond order metals such as Fe, Ti and Zr, but small in the high C–1st bond order metals such as Nb and Mo. This difference in the bond order ratio from one BCC metal to the others may be associated with the tendency for the occurrence of allotropic transformation in them. For example, BCC Fe transforms to FCC Fe, and BCC Ti and Zr transform to HCP Ti and Zr, but neither Nb nor Mo shows such a phase transformation. Thus, there is a trend that the magnitudes of the second-nearest-neighbour interactions are large in those BCC metals which exhibit an allotropic transformation to the close-packed phase (FCC or HCP) at certain temperatures [17]. Geometrically, in the close-packed phase (FCC or HCP) an atom is surrounded by 12 first-neighbour atoms. In the BCC phase an atom is surrounded by 14 atoms, if the second-nearest neighbours are included, as shown in figure 1(*b*). The present calculation implies that the BCC metal, on transforming to the FCC (or HCP) phase, tends to hold the FCC-like (or HCP-like) atomic interaction even in the BCC phase. In other words, in such a BCC metal, the attractive atomic interactions operate over the first and second neighbours as if the metal has a higher coordination number such as FCC or HCP.

The heat of transformation [27] is much lower in Fe than in Zr and Ti, as is shown in figure 14. This means that the allotropic transformation takes place more easily in Fe than in Ti and Zr. It is also known that BCC Y transforms to HCP Y, and its heat of transformation is the largest of a variety of metals so far reported [27]. It is evident from figure 14 that there was no allotropic transformation in those metals which have a bond order ratio smaller than a certain critical value. This critical value may be assumed to be the value at the point where the broken line in the figure crossed the heat of transformation line for Y. For example, V, with the bond order ratio of 0.15, has no allotropic transformation. Both Nb and Mo have even lower bond order ratios than V. It is also true that both Nb and Mo have very high total bond orders in the BCC state, as shown in figure 12(a). Thus, Nb and Mo are very stable in the BCC state, and the second-nearest-neighbour interaction is less marked than those of other BCC metals.

5. Conclusions

The electronic states for Nb and Mo containing a variety of alloying elements were calculated systematically by the DV-Xα cluster method. The activation energies for impurity diffusion

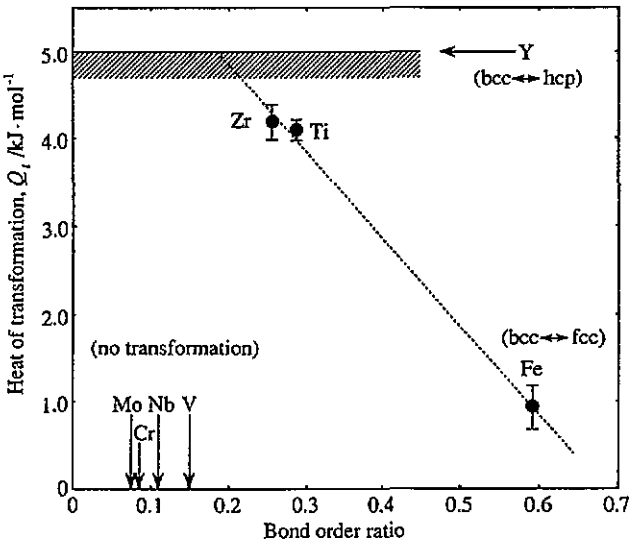

Figure 14. Correlation of the heat of transformation of BCC metals with the bond order.

and self-diffusion were found to correlate with the bond order. Also, both the Nb and the Mo binary phase diagrams could be classified using the BO–MD map. Moreover, structural stability was compared for Nb, Mo and other BCC metals using either the bond order or the bond order ratio. Thus, it is concluded that the new alloying parameters BO and MD are useful in describing the alloying behaviour of Nb and Mo.

Acknowledgments

The authors acknowledge the Computer Center, Institute for Molecular Science, Okazaki National Institutes for the use of the HITAC M-680H and S-820 computers. This research was supported in part by the Grant-in-Aid for Scientific Research from the Ministry of Education, Science and Culture of Japan.

References

[1] Lampman S R and Zorc T B (ed) 1990 *Metals Handbook* vol 2, 10th edn (Metals Park, OH: American Society for Metals) p 557
[2] Kato M, Kano S, Inoue S, Isshiki Y, Saito J, Yoshida E and Morinaga M 1993 *J. Japan Inst. Met.* **52** 233
[3] Ellialtioglu S, Zeller R and Dedrichs P H 1987 *J. Phys. F: Met. Phys.* **17** 409
[4] Matthias R T, Peter M, Williams H J, Clogston A M, Corenzwit E and Sherwood R C 1960 *Phys. Rev. Lett.* **5** 542
[5] Clogston A M, Matthias B T, Peter M, Williams H J, Corenzwit E and Sherwood R C 1962 *Phys. Rev.* **125** 541
[6] Postnikov A V, Anisimov V I and Gubanov V A 1983 *J. Magn. Magn. Mater.* **39** 295
[7] Podloucky R, Deutz J, Zeller R and Dederichs P H 1980 *Phys. Status Solidi* b **112** 515
[8] Lang P, Drittler B, Zeller R and Dedrichs P H 1992 *J. Phys.: Condens. Matter* **4** 911
[9] Nakao Y and Wakoh S 1987 *J. Phys. Soc. Japan* **56** 3983
[10] Jani A R, Brener N E and Callaway J 1988 *Phys. Rev.* B **38** 9425
[11] Jani A R, Tripathi G S, Brener N E and Callaway J 1989 *Phys. Rev.* B **40** 1593

[12] van Ek J and Lodder A 1991 *J. Phys.: Condens. Matter* **3** 7363
[13] Miedema A E 1973 *J. Less-Common Met.* **32** 117
[14] Chelikowsky J R 1979 *Phys. Rev.* B **19** 686
[15] Morinaga M, Yukawa N and Adachi H 1984 *Bull. Japan Inst. Met.* **23** 911
[16] Morinaga M, Yukawa N and Adachi H 1985 *Tetsu-to-Hagane* **71** 1441
[17] Morinaga M, Yukawa N and Adachi H 1985 *J. Phys. F: Met. Phys.* **15** 1071
[18] Morinaga M, Yukawa N, Maya T, Sone K and Adachi H 1988 *Proc 6th World Conf. on Titanium* (Paris: Société Française de Métallurgie) p 1601
[19] Morinaga M, Yukawa N and Adachi H 1988 *Bull. Japan Inst. Metals* **27** 165
[20] Morinaga M, Yukawa N, Ezaki H and Adachi H 1985 *Phil. Mag.* A **51** 223
[21] Morinaga M, Yukawa N, Ezaki H and Adachi H 1985 *Phil. Mag.* A **51** 247
[22] Slater J C 1979 *The Calculation of Molecular Orbitals* (New York: Wiley)
[23] Averill F W and Ellis D E 1973 *J. Chem. Phys.* **59** 6413
[24] Mulliken R S 1955 *J. Chem. Phys.* **23** 1833, 1841, 2338, 2343
[25] Satoko C, Tsukada M and Adachi H 1978 *J. Phys. Soc. Japan* **45** 1333
[26] Morinaga M, Yukawa N and Adachi H 1984 *J. Phys. Soc. Japan* **53** 653
[27] Japan Institute of Metals 1993 *Metals Data Book* (Tokyo: Maruzen) 11, 20
[28] Weast R C (ed) 1989 *Handbook of Chemistry and Physics* 70th edn (Boca Raton, FL: CRC Press) p F-54
[29] Massalski T B (ed) 1990 *Binary Phase Diagrams* vol 1–3, 2nd edn (Metals Park, OH: American Society of Metals)
[30] Pauling L 1960 *Nature of the Chemical Bond* 3rd edn (Ithaca, NY: Cornell University Press)